Accepted Manuscript

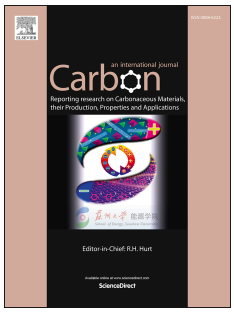

Chirality-independent characteristic crystal length in carbon nanotube textiles measured by Raman spectroscopy

John S. Bulmer, Thurid S. Gspann, Jon S. Barnard, James A. Elliott

PII: S0008-6223(17)30054-4

DOI: 10.1016/j.carbon.2017.01.044

Reference: CARBON 11653

To appear in: *Carbon*

Received Date: 9 July 2016

Revised Date: 10 January 2017

Accepted Date: 14 January 2017

Please cite this article as: J.S. Bulmer, T.S. Gspann, J.S. Barnard, J.A. Elliott, Chirality-independent characteristic crystal length in carbon nanotube textiles measured by Raman spectroscopy, *Carbon* (2017), doi: 10.1016/j.carbon.2017.01.044.

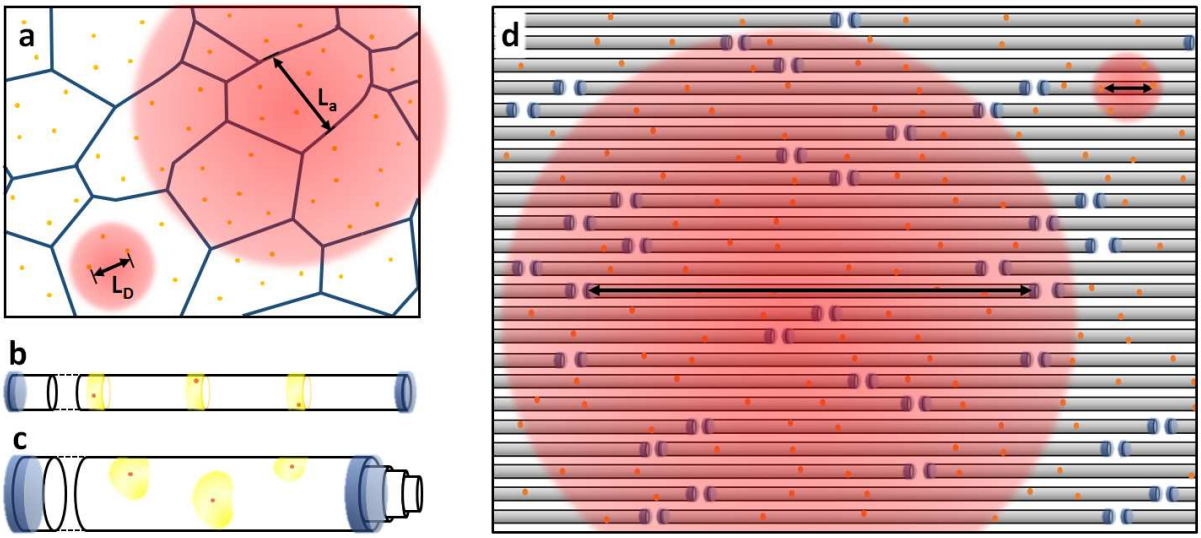

Chirality-Independent Characteristic Crystal Length in Carbon Nanotube Textiles measured by Raman Spectroscopy

John S. Bulmer*, Thurid S. Gspann, Jon S. Barnard, James A. Elliott
Department of Materials Science and Metallurgy, 27 Charles Babbage Road, University of Cambridge, CB3 0FS, UK

Raman spectroscopy's D:G ratio is a well-known indicator of graphitic crystallinity in single-wall carbon nanotubes (SWCNTs) with widespread qualitative application to macroscopic CNT assemblies. Here, we show how the D:G ratio yields quantitative characteristic crystal length features that is remarkably independent of SWCNT chirality when purified SWCNTs are in a high density, heavily bundled textile form. Purified, unaligned, SWCNT films of enriched length distributions and controlled chirality responded in ways consistent with power law behaviour, where the D:G ratio is proportional to the fourth power of excitation wavelength, inversely proportional to SWCNT length, and fits to a master curve independent of electronic species concentration. This behaviour, matching the established response of graphite and graphene, unexpectedly persists despite complications from chirality-dependent resonances unique to SWCNTs. We also show that textiles comprising of aligned, long length CNTs defy these simple power laws until defective multiwall CNTs and impurities are removed post-process, and only if sample heating under the Raman laser is minimized. Adjusting the Raman laser beam diameter up to 6 mm, which is well beyond the average CNT length, we propose that the CNT textile's characteristic crystal length is the CNT length or, with point defects, the distance between point defects.

*Corresponding Author: jb833@cam.ac.uk (John Bulmer)
+44 1223 334300

1. Introduction

Similar to graphitic intercalation compounds [1] and conductive polymers [2], the electrical conductivity of textiles based on single wall carbon nanotubes (SWCNTs) is dependent on their crystallinity [3] [4]. Graphitic crystallinity, or the degree of order in the sp^2 lattice, is often gauged by considering the D to G ratio, a widespread metric in Raman spectroscopy that divides the intensity of the Raman D peak with the intensity of the Raman G peak. The G peak, centred at approximately 1580 cm^{-1}, is a prominent feature in graphitic materials and is related to the tangential vibration modes of sp^2 bound carbon atoms. The D peak is related to defects that break the translational symmetry in an sp^2 plane and is centred at approximately 1320 cm^{-1}, although its exact position is dependent on laser excitation wavelength [5] [6] [7]. D:G ratios vary considerably between different CNT materials. Many multiwall CNT based materials have D:G ratios ranging from 0.27 to 0.9 [8] [9], even after a graphitizing annealing (>2000°C) post-process [10]. SWCNTs and double wall CNTs typically have better D:G ratios [3] [4] [11]. After a post-process purification, for example, double wall CNT textiles produced by our group experience an enhanced D:G ratio from 0.09 as-is to 0.01 purified (for 532 nm laser excitation) and from 0.12 as-is to 0.04 purified (for 785 nm laser excitation). These improved D:G ratios qualitatively indicate enhanced purity and crystallinity although by themselves do not shed light on physical parameters or the exact mechanism inducing the improvement.

In this report, we study the D:G ratios of highly purified, unaligned SWCNTs in a bulk film morphology where the average SWCNT length and electronic species concentration have been enriched by density gradient ultracentrifugation and are known. This results in a robust methodology for determining a characteristic crystal grain dimension in a bulk CNT textile, *independent of the electronic species concentration and chirality dependent resonances*. For graphite and graphene, this is an established technique where spatial grain characterization is more straightforward [7] and chirality dependent complexities are not a factor. For CNTs, systematic characterization of D:G against crystal grain length on isolated SWCNTs is scarce [12] [13] [14] and, until now, seemingly non-existent in heavily bundled, dense textile morphologies. Further, these past studies on *isolated* SWCNTs were composed of the standard uncontrolled, mixed electronic species. They showed chirality dependent behaviour where metallic SWCNTs and semi-conducting SWCNTs in the same film resonate at different Raman

excitation wavelengths. This leads to a non-monotonic relationship between the D:G ratio and Raman excitation wavelength. In our *dense* SWCNT films of *enriched* electronic species concentration (predominately metallic, semi-conducting, and unsorted SWCNTs), we unexpectedly find that the D:G ratio dependence on wavelength is the same response known for graphite and graphene. Armed with this finding, we examine aligned CNT textiles made by our in-house reactor where there is less control on CNT length and electronic species concentration, although it may be manufactured on an industrial scale. We use a post-process purification step to improve the D:G ratio and find that the D:G response with wavelength resembles graphite or graphene only after the purification step.

We also investigated the effect of the excitation laser spot size on the D:G ratio. Typical laser spot sizes on Raman microscopes are at their largest tens of microns, which is substantially smaller than the average length of CNTs in our in-house manufactured textiles. We used a specially designed Raman probe that generates a 6 mm beam spot, considerably exceeding the average CNT length, to determine whether a larger relative spot yields a more accurate defect sampling and D:G value.

The intent of this report is to not expand on the origin of the D peak, but to better understand the circumstances making the Raman D:G ratio a more quantitative measurement for dense CNT textile manufacturing. In the following we will show: 1) For the dense CNT textiles considered here, the D:G relationship with excitation wavelength appears to be the same as the known relationship in graphite and graphene, with chirality or electronic species concentration never significantly affecting the D:G ratio. 2) The D:G ratio of dense SWCNT films with sorted electronic species concentrations and enriched SWCNT length distributions fit into a master curve independent of electronic nature. 3) This technique may be useful for the development of CNT textiles to probe characteristic crystal length, although only after sufficient purification. 4) While not observed with the current CNT materials, a Raman laser spot larger than the average CNT length may eventually become necessary to accurately characterize a CNT textile.

2. Background

2.1 Simple geometrical origin of the D:G to length relationship. For many researchers primarily interested in growing and using bulk *sp*2 carbon materials, the D:G ratio is an simple, quick and non-destructive metric that empirically blends material purity [8] [15] and atomic crystal quality [12] [13] [16] into a single scalar indicator. In the 1970s, the first Raman measurements on graphite qualitatively observed the D:G effect that relates the D:G ratio to the average graphitic crystal grain length, L_a [5] [7] [17]:

$$D:G = \frac{C_1(\lambda)}{L_a} \tag{1}$$

where $C_1(\lambda)$ is a parameter dependent on the excitation laser wavelength λ. For graphite and graphene, multiple laser line measurements indicated that $C_1(\lambda) \propto \lambda^4$ [5] [18]. Other sp^2 carbon species, such as amorphous carbon, disordered graphite, carbon foams, and CNTs have shown more a complicated dependence of the D:G ratio on wavelength [13] [19] [20].

While the past forty years have seen practical utilization of D:G ratio characterization in many carbon types, the fundamental origin of the D peak has only relatively recently reached a mature understanding [5] [7]. A localised (~3 nm) zone of sp^2 carbon around a graphene defect contributes the most to the D peak signal and not the defect itself [5] [7] [21]. As explained in [5] [7] and illustrated in figure 1a, this fact enables a simple geometrical derivation of (1) in graphite and graphene: The D peak from the total graphene crystal grain scales with the crystal perimeter and resultantly $D \propto L_a$, the average graphitic crystal grain length. It is known that the G peak signal depends on the crystal grain area, therefore $G \propto L_a^2$. As a result, $D:G \propto L_a^{-1}$ as expected from the empirically determined (1). When the Raman laser beam is smaller than the crystal grain and the crystal grain boundary is not captured, a sparse defect situation occurs with an average distance L_D between sparse point defects. Using similar geometrical arguments, D scales for a given defect density with the laser spot area $(d_{Laser}/L_D)^2$, while G scales with the illuminated area d_{Laser}^2; (1) is modified according to $D:G \propto L_D^2$ (see figure 1a).

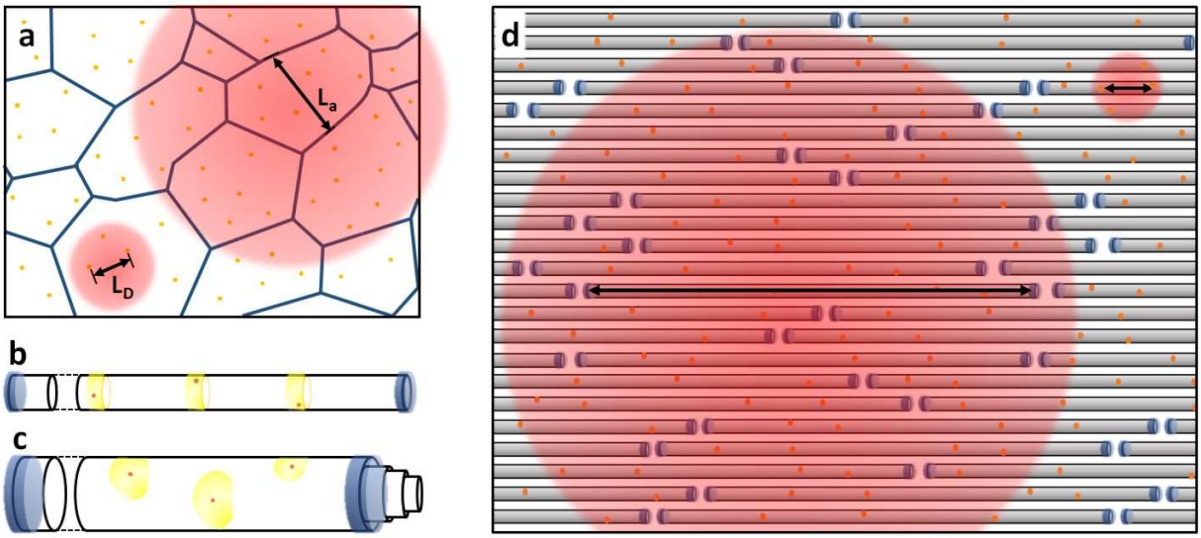

Figure 1| a, Illustration of the two well-established situations in which defects collectively add to the D peak signal in crystalline graphite and graphene. The large red shaded region represents situation 1 where the Raman laser beam probes defects from grain boundaries and point defects in the lattice. The sparse defect situation, situation 2, is represented by the small, red shaded region where the Raman laser spot is significantly smaller than the graphitic crystal grains and point defects are the primary contribution to the D peak signal. **b & c,** Illustration of two proposed situations in which defects collectively add to the D peak signal in crystalline CNTs: **b**, point defects on the one dimensional structure act as crystal grain boundaries; **c**, a sparse defect situation, particularly suited for large diameter CNTs, where point defects no longer define a boundary. **d,** Illustration of a CNT assembly where the Raman laser beam is smaller than the average CNT length (small red shaded region) and does not accurately sample the D:G contribution from CNT ends. A Raman beam much larger than the CNT length (large red shaded region) would accurately sample the D:G of the full material.

2.2 Geometrical D:G extension to CNTs. Equation (1) primarily concerns graphite and graphene and their application to cylindrical CNTs is somewhat ambiguous. First, SWCNT absorption in the visible spectrum is governed by electronic transitions between van Hove singularities and this makes the Raman spectra chirality dependent. This is a feature unique to SWCNTs, which does not exist in graphite. One study [13] showed that D:G ratio decreases with wavelength, reaching a minimum at 620 nm (2 eV), and then increases. This non-monotonic behaviour was attributed to chirality-dependent effects where the metallic SWCNT fraction began to particularly resonate at smaller excitation wavelengths. Note, however, that this study was with SWCNTs isolated from each other using a DNA wrapping technique and not in the interacting bundled form found in textiles. Another early study [22] on bulk SWCNT films measured the D:G ratio against Raman excitation wavelength and also found a non-monotonic

response. While this study considered several sources of SWCNTs, they did not mention any post growth purification processes and it is very likely amorphous carbon and other impurities complicate the D peak signal.

Another challenge when applying (1) to SWCNTs is that a two dimensional crystal grain is not well defined for something largely treated as a one dimensional object. Several studies [12] [13] [14] characterized the D peak against average CNT length and found the expected inverse length proportionality, indicating CNT ends act as crystal grain boundaries. Note that the SWCNT mentioned here are in a liquid suspension or sparse networks, and not the heavily bundled textiles we consider in our study. Both optical and electronic properties of SWCNTs are different in an isolated versus a bundled state [23] [24] [25].

While experimentally verified in these sparse CNT networks, it was assumed the CNT length was analogous to the crystal grain size in graphite [12] [13] [14] without specific discussion why this would be the case. Here, we consider the simple, established geometrical argument for D:G in graphite and extend it to CNTs. Consider the edge of the rolled graphene plane at the ends of the CNT as a CNT "grain boundary." This is the obvious case for open endcaps and the same applies to closed endcaps where a ring of Stone-Wales defects closes the CNT structure [26]. Hence the amount of defects scales with CNT circumference and $D \propto d_{CNT}$, where d_{CNT} is the CNT diameter. The sp^2 lattice area exposed to the laser dictates the G peak magnitude, or $G \propto d_{CNT}\ L_{CNT}$ where L_{CNT} is the CNT length. Thus, $\mathrm{D{:}G} \propto L_{CNT}^{-1}$ for individual CNTs as experimentally verified in aforementioned Raman studies on sparse networks of CNTs.

Beyond CNT ends, single point defects could create a crystal grain boundary in effectively one dimensional CNTs (Figure 1b). As discussed in [5] [7] [21], a point defect in graphene has a ~3 nm sp^2 zone around it that is the primary contribution to the D peak signal. This is likely the case for CNTs and, while the size of this proposed sp^2 zone around a CNT defect is not known, it is possible the zone wraps back on itself making the entire circumference contribute to the D peak signal. In this case, the D peak signal also scales with d_{CNT} and point defects and endcaps look similar as far as Raman spectroscopy is concerned. Further, the unavoidability of scattering of charge carriers from point defects in one dimensional structures makes them analogous to transport across crystal grains in graphene. Past experiments in double-walled CNT films, made

defective through ion bombardment, experienced an increased D:G ratio. This D:G increase was attributed to an increase in point defects and these point defects were shown to define CNT crystal grain boundaries [27].

In contrast, for large diameter multiwall CNTs and large SWCNT bundles where transport is governed by two spatial coordinates, point defects would possibly *not* serve as crystal grain boundaries (Figure 1c). This permits charge carriers to manoeuvre around point defects and this now enables a circumstance analogous to graphene's sparse defect situation, where the D peak contribution comes from point defects and not grain boundaries. A possible example would be our in-house produced CNT textiles where the laser spot (typically tens of microns) is significantly smaller than the average CNT bundle length (up to millimetres [28]). Now, consider the case for an individual long CNT where the D peak contribution now comes purely from counting sparse point defects. Thus, $D \propto (d_{Laser}/ L_D)$ where L_D is average distance between sparse defects and d_{Laser} is the diameter of the laser spot. Because the CNT is effectively one dimensional, $G \propto d_{Laser}$ and this makes $D:G \propto L_D^{-1}$. Note this is a dissimilar result to sparse defect graphite, where $D:G \propto L_D^{-2}$.

For an n number of CNTs in an aligned array, for both the CNT endcap and sparse defect situations, the signal strength of both the D and G peaks scales with n. As a result, the derived D:G relationships are not changed by being in an aligned array. Thus, in a way that parallels the D:G derivation in graphite [5] [7], there are three limiting D:G scenarios for CNTs: 1) CNT ends act as graphitic crystal grains boundaries and, depending on CNT diameter and size of the defect zone, either 2) point defects act as crystal grain boundaries too, or 3) point defects act as sparse contributors. In all three scenarios:

$$D:G = \frac{C(\lambda)}{L} \tag{2}$$

where $C(\lambda)$ is to be determined and L is the characteristic length between crystal grain boundaries. When crystal grains are not significant in the material, such as when the laser spot is much smaller than the CNTs, we speculate that L becomes the average length between sparse defects. If the sparse defect situation is relevant in CNTs, it may be possible to see a sparse

defect dominant situation transform to a crystal grain dominant situation with a sufficiently large laser beam diameter (Figure 1d).

3. Experimental Methods

3.1 Materials. This paper considers two sources of CNT textiles. The first source is freestanding, unaligned SWCNT buckypaper samples commercially obtained from *NanoIntegris* where the average SWCNT length and electronic species concentration is enriched and known. These SWCNT films were generated by the arc discharge process where the company reported purity levels of the final product generally were below 5% for amorphous carbon and 1% for iron catalyst by weight.

Three *NanoIntegris* unaligned SWCNT films of the typical unsorted variety were considered where their individual length distributions were: long length (1030 +/- 667 nm), medium length (315 +/- 100 nm), and short length (233 +/- 67 nm). *NanoIntegris* altered the average SWCNT length by sonicating the SWCNTs in suspension and then measuring them with an automated Veeco DI EnviroScope atomic force microscope using standard techniques [29]. Histograms of the SWCNT length distributions are shown in supplemental information, figure S1.

Three other *NanoIntegris* SWCNT films were considered where density gradient separation [30] controlled the electronic species concentration with the following levels: a metal film (95% metallic SWCNTs (average length 763 +/- 473 nm), a semi-conducting film (99% semi-conducting SWCNTs, average length 906 +/- 467 nm), and a chiral film (99% semi-conducting SWCNTs of predominantly one chirality, same length distribution expected as the previous film). Metallic SWCNT enrichment was measured with calibrated UV/vis absorption spectroscopy. The calibration was accomplished according to [31] where the absorption signal was associated with directly counting CNTs with a bandgap. For the chiral film, the exact concentration of the chiral enrichment is unknown. Qualitatively, however, its absorption peaks in the UV/vis absorption spectrum are substantially more narrow and defined relative to the un-enriched semi-conducting film (See supplemental information, figure S2). Scanning electron

microscopy shows the micro-structure of the unaligned SWCNT bundles (See supplemental information, figure S4 and S5). At this scale, however, differences in the films with various length distributions and electronic species concentrations were not apparent. Qualitative confirmation of the overall electronic nature of the sorted films was accomplished with cryogenic transport measurements (See supplemental information, figure S3).

The other material considered, a freestanding textile composed of roughly aligned, long length CNTs, was made in-house using the floating catalyst chemical vapour deposition process. The process is described elsewhere [28], although briefly ferrocene, thiophene, and a carbon source (such as toluene or n-butanol [32]) are vaporized and injected into a 1300°C tube furnace with hydrogen carrier gas. This results in CNT formation in a floating aerogel. The aerogel is directly pulled out of the reactor by mechanical means where the speed of extraction dictates the degree of internal microstructure alignment. The precise length of these CNTs is not known, although some transmission microscopy studies indicate they approach and are no longer than 1 mm [28]. This internal length is significantly longer than the *NanoIntegris* material, as well as the laser spot size from typical Raman microscopes. Note that these textiles have more impurities than the *NanoIntegris* material. Amorphous or oligomeric carbons are typically ~10% of the total weight and catalytic impurities are typically 5-15% of the total weight as measured by thermo-gravimetric analysis. Scanning electron microscopy and transmission electron microscopy shows the bundles and micro-structure (See supplemental information, figures S6 to S14). Bundles of double wall CNTs and SWCNT are present as directly observed and indicated by electron diffraction analysis in the microscope. This is also substantiated by the radial breathing modes in the Raman spectra (See supplemental information, figure S16). Also shown in the microscopy are larger, malformed multiwall CNTs and other disordered carbons that were common in the assembly. As described in the supplemental information figure S15, polarized Raman spectroscopy did find anisotropy in the as-is textile and this suggests microstructure alignment. The intensity of the G peak increased a factor of three as both the Raman excitation laser polarisation and the analyser of the Raman scattered light changed from perpendicular to parallel to the spinning direction.

We purified our in-house CNT textiles with a post-process purification that will be described in another report. As observed by scanning electron microscopy (See supplemental information,

figures S6 to S9), the purification results in the selected removal of multiwall CNTs and other malformed carbon structures, and leaves behind highly aligned, predominantly double wall CNT bundles. This is substantiated in transmission electron microscopy by the dramatic removal of carbon species that are either irregularly shaped or have a large tubular structure with a core, as shown in the before and after pictures of figures S10 to S14 of the supplemental section. Electron diffraction analysis on individual CNTs not part of a bundle showed they were mostly double wall CNTs after purification. While the prevalence of the individual double wall CNTs are an indication of the whole, it cannot be guaranteed that the few walled CNTs shown in bundles are exclusively double walls too. These microscopy images show significant iron catalyst residue on the surface, and while this residue may be easily removed with wet chemistry techniques, the Raman measurements presented here were typically conducted without this step. As shown in the supplemental section figure S15, polarized Raman spectroscopy of the purified textiles shows considerable anisotropy of the G peak signal (a factor of ten) when measured parallel and perpendicular the spinning direction. As will be shown in the results section, the Raman D:G ratio improves significantly after the purification process, across all Raman excitation wavelengths, while the radial breathing modes are unaffected. This high degree of the crystallinity improvement is the initial motivation for this Raman study. The substantial suppression of the D peak and unaltered perseverance of the radial breathing modes is another indicator that the purification process removes multiwall CNTs and other malformed carbon structures, which are known to have substantially larger D peak signals than few walled CNTs. There are other established methodologies for similar purification [33] [34] [35] [36] [37]. The point of this report is not the purification process itself, but the fact a high degree of graphitic crystallinity and species homogeneity may be required in CNT textiles before the λ^4 relationship applies and may be used to characterize the material.

3.2 Raman spectroscopy. Raman spectroscopy was primarily accomplished with a Bruker Senterra Raman microscope with three laser lines: 532, 633, and 785 nm. The D:G ratio is a polarization-dependent quantity [7] and unless otherwise stated the lasers were depolarized. Raman measurements were accomplished on five or more locations on a given material and, after normalizing to the G peak, yielded an average spectrum. The standard deviation between these points was used to calculate error bars. D:G analysis was accomplished by selecting the D:G spectrum region (~1100 to ~1700 cm^{-1}) and applying a baseline correction in *Opus*

software. To calculate the D:G ratio, simply selecting the D and G peak height intensities did not lead to meaningful trends. Instead, the D:G ratio was calculated by integrating the peak area. Area integration is a better methodology for crystalline graphitic materials [21] and yielded consistent power law behaviour.

If not properly mitigated, sample heating under the laser caused reversible broadening of the G peak. This leads to an inaccurate D:G value and is an effect that has been observed before [38] [39] [40]. In the results section, we will show a proportionality between the D:G ratio and excitation wavelength to the fourth power, λ^4. When reversible heating is a factor, this proportionality apparently remains, except a non-zero intercept shifts the line vertically. To mitigate heating, we used the largest microscope objective available (4× with ~10 µm spot size) and lowest practical laser fluence parameters (intensity, collection time, and accumulation number). This ensured the G peak spectrum was largely fluence independent while still permitting a sufficiently defined D peak. We found this careful control of fluence zeroed out the vertical intercept when plotting the D:G ratio against λ^4. Effective laser parameters under the 4× objective (0.1 N.A.) are: 532 nm: 2 mW/ 4 s/ 3 accumulations; 633 nm: 2 mW/ 5 s/ 2 accumulations; 785 nm: 1 mW/ 10 s/ 2 accumulations.

Spectra were also obtained with a Kaiser Raman spectrometer (randomly polarized, 785 nm laser line) with a PHAT system probe head, a special fiber optic enabled device that captures greater Raman scattered light with a substantially larger solid angle collection. This permits use of a 6 mm excitation laser beam diameter, which we will use to search for intrinsic differences between the relative laser beam diameter and average SWCNT length. Typical laser parameters here are 400 mW/ 30 s/ 2 accumulations, approximately thirty thousand times smaller fluence than the 4× objective.

4. Results

4.1 Length enriched, unaligned SWCNT film. Now we discuss the results of the unaligned *NanoIntegris* SWCNT film with different length distributions. Figure 2 shows a representative spectrum without baseline subtraction, in this particular case for the film of the shortest SWCNT

length (Other spectra are in the supplemental information, figures S16 to S22). The black trace is the signal and red is the standard deviation showing good repeatability between multiple measurement locations. In general, these SWCNT spectrums are archetypal: chirality dependent radial breathing mode peaks at the spectrum's lowest energy and the D peak overtone at the highest energy. In the spectrum's middle are the D and G peaks which are central to this study.

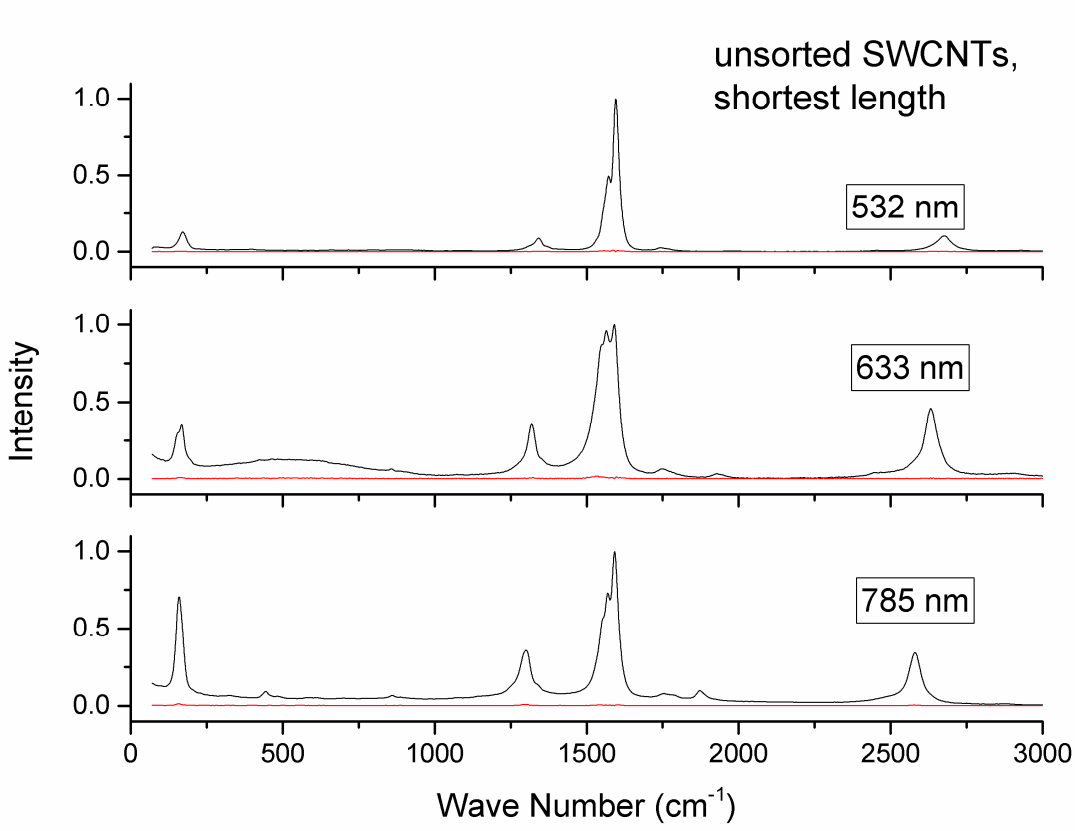

Figure 2| Raman spectra of the unsorted, unaligned SWCNT film, composed of the shortest length SWCNTs (233 +/- 67 nm) under three laser lines. The D peak grows with wavelength while the G peak structure has a complicated relationship with wavelength.

As shown with the three different wavelengths, the D peak gets taller and wider with the laser wavelength in a simple, monotonic fashion. The G peak, on the other hand, has a substantially different structure between excitation wavelengths and, in particular, becomes broader for the 633 nm excitation. Similar broadening of the G peak with different wavelengths has been seen before in SWCNT films [22]. The radial breathing modes, which are chirality dependent effects unique to CNTs, also are shown to depend on wavelength. These chirality dependent effects are present in all the materials considered (See supplemental information, figures S16 to S22).

Considering that 1) chirality resonant effects are present, and 2) a seemingly non-monotonic G peak relationship exists with wavelength, at this point a simple D:G ratio relationship with Raman excitation wavelength seems unlikely.

Figure 3 shows the D:G values of all three unsorted films, plotted against excitation wavelength to the fourth power, λ^4. As shown there is good linear proportionality between these parameters, which is the same response as graphite and graphene [5] [7] [18]. We observe that the films of shorter SWCNTs yield higher slopes, which is a negative correlation with length as predicted by (2). The negative correlation between these slopes and SWCNT length distributions are an indication that SWCNT length may indeed be inferred in a bulk material with different Raman laser excitations. Note that this proportionality between D:G ratio and λ^4 is maintained despite the demonstrated resonant, chirality dependent behaviour at different wavelengths (particularly the broadening of the G peak at 633 nm). This is a non-trivial response and implies that, as the G peak area grows and shrinks with wavelength, the D peak grows in a way to maintain the λ^4 proportionality. As discussed in the background, *isolated* SWCNTs displayed more complicated, non-monotonic behaviour where D:G ratio first decreases with wavelength and then, due to resonant chirality dependent effects, begins to increase with wavelength [13]. However, it is well known that bundled SWCNTs, as opposed to individual SWCNTs, have broader and more red shifted features in both Raman and absorption spectroscopy [23] [24] [25]. If phonon-phonon coupling is sufficiently strong between SWCNTs in a bundle, chirality dependent resonant perturbations could dampen to the point where the bundle's response approaches the behaviour of graphite.

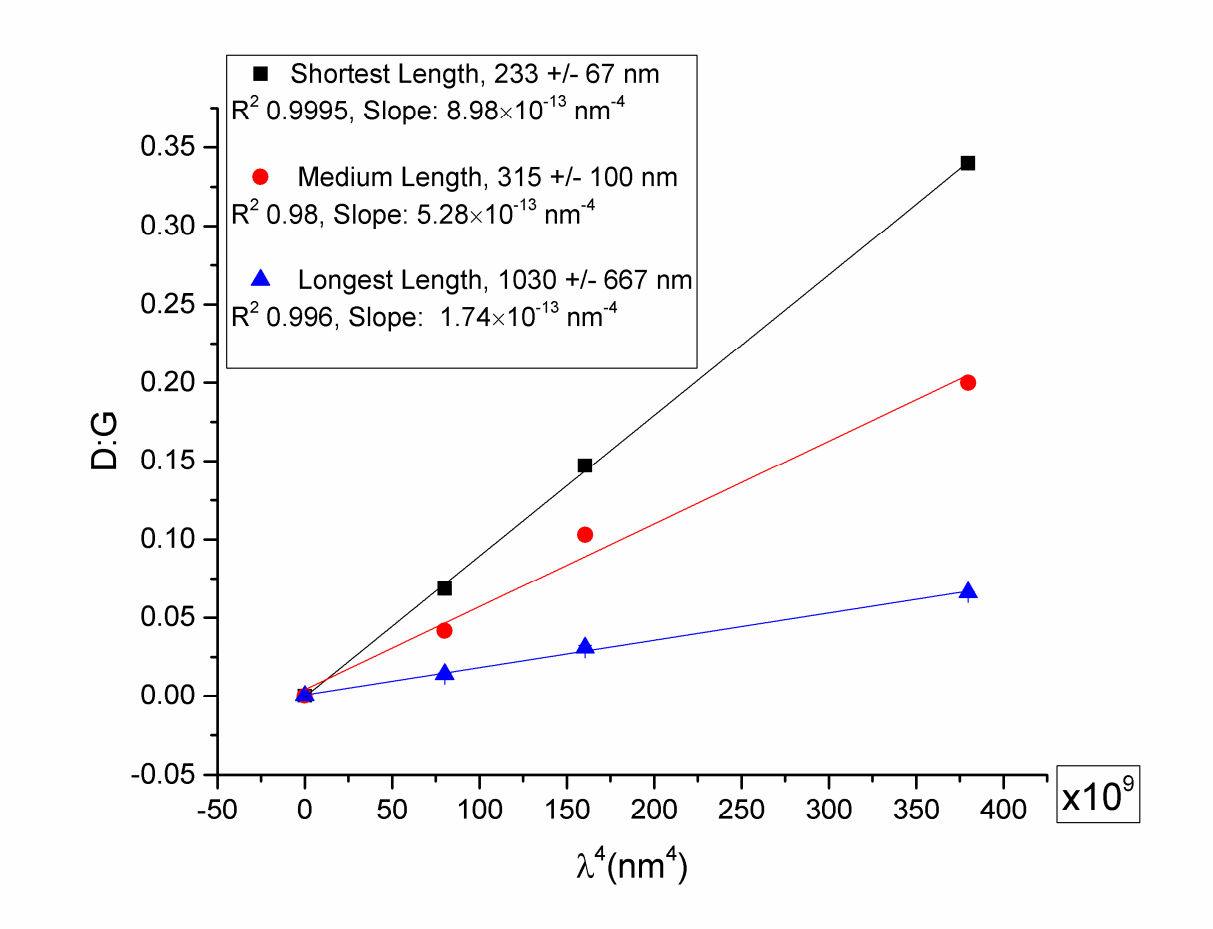

Figure 3| Dependence of the D:G values on wavelength to the fourth power, λ^4, for all three unsorted SWCNT films of different length distributions. Good linearity is maintained despite observing chirality dependent resonant conditions under different laser lines.

Figure 4 shows the D:G ratios of the three unsorted films plotted against the inverse of their average lengths. By virtue of the material preparation, there is unavoidable and substantial variance in the length and it is desirable to fix as few of the fitting parameters as possible. Therefore, the data is presented on double logarithmic axes, where linearity indicates power law behaviour and the fitted slope is the exponent associated with the power law. While the error bars are large and could support a range of slopes, there is at the very least a positive correlation between these parameters and the best slope fits give a power law exponent of unity. This is the case for every wavelength used. Considering that past studies [12] [13] [14] on *isolated* SWCNTs also had the same unity exponent, these best fits here are consistent with past results and what was predicted in equation (2). This supports that, as CNT length is the known

characteristic crystal length *L* in isolated CNT networks, this may also be the case in dense CNT textiles.

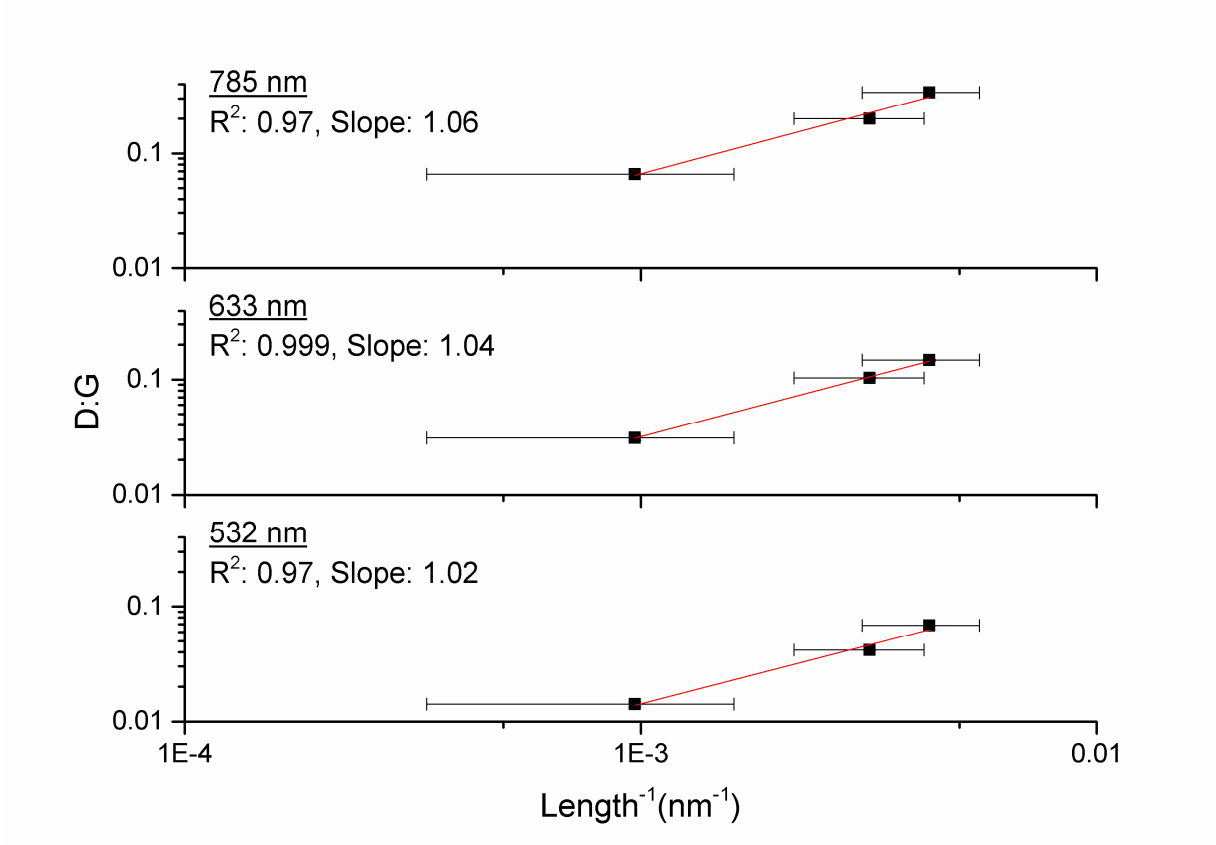

Figure 4| Log-log plot of D:G values plotted against the inverse of average length for each unsorted SWCNT film. Linearity here indicates a power law with the slope indicating the appropriate exponent for the inverted length. The best fit slopes for each wavelength equals ~1, which is consistent with equation (2).

To further access the validity of equation (2), we plot D:G λ^{-4} versus the inverse of CNT length to collapse all the depicted curves into a single master curve (Figure 5). The same approach was taken with characterizing nano-crystalline graphite [18], as depicted. Indeed, a master curve is generated showing SWCNT adherence to equation (2) with proportionality to λ^4, within the margin of error.

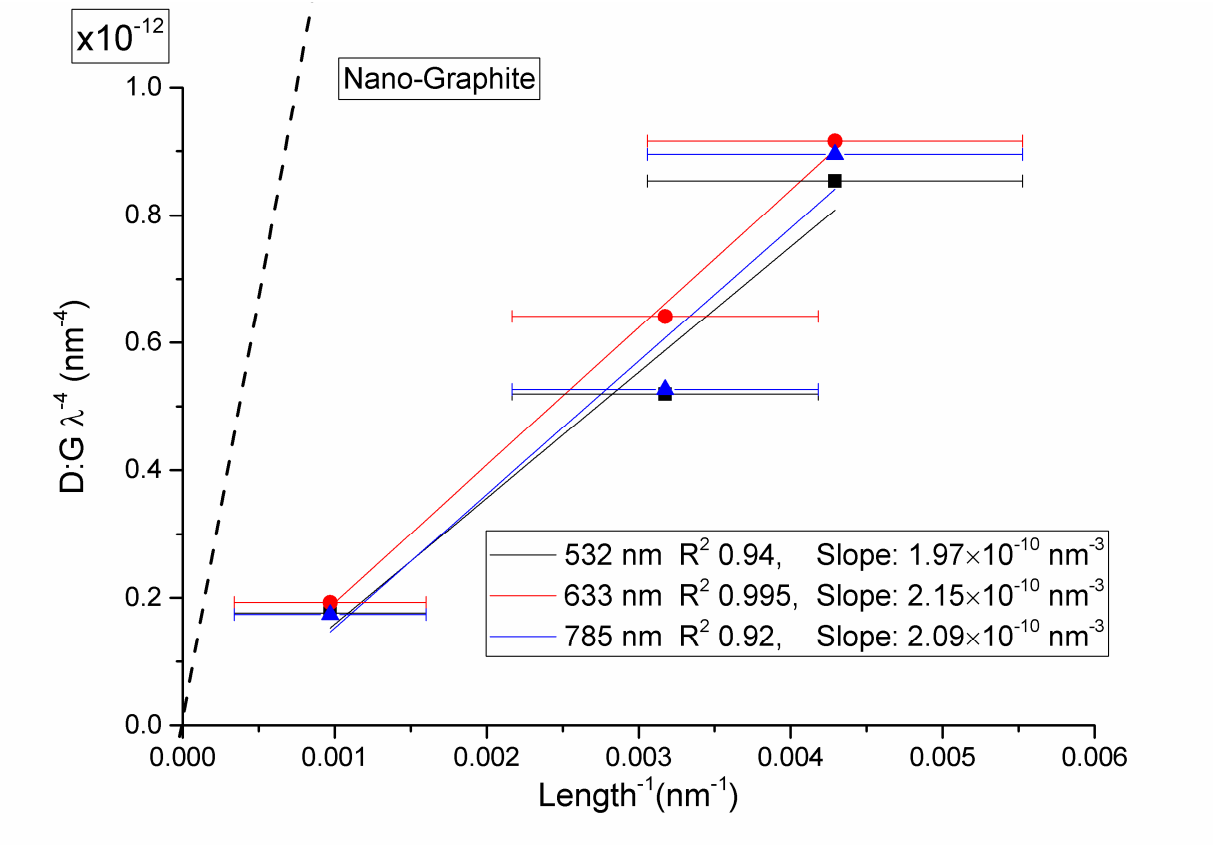

Figure 5| A master curve of the unsorted SWCNT films incorporating all D:G values, lengths, and wavelengths. As a reference, the published master curve for nano-crystalline graphite is provided [18].

4.2 Electronic species controlled, unaligned SWCNT films. For the metallic, semi-conducting, and chiral films, figure 6a shows the same λ^4 proportionality as we found for the unsorted, length enriched films. Further, the metallic SWCNTs have the largest slope, which is expected because they have the shortest length. Figure 6b plots their D:G ratios with the master curve. Surprisingly, despite their distinct electronic species concentrations, we find these materials also reside on the unsorted SWCNT master curve within the margin of error. This is particularly noteworthy for the metallic SWCNTs, which are typically known to have higher D:G ratios [7]. This suggests that in a bulk state, electronic species concentration plays less of a role in the D:G ratio dependence on length and wavelength. As methods develop to generate films with tighter CNT length tolerances, the universality and applicability of these master curves may be better explored.

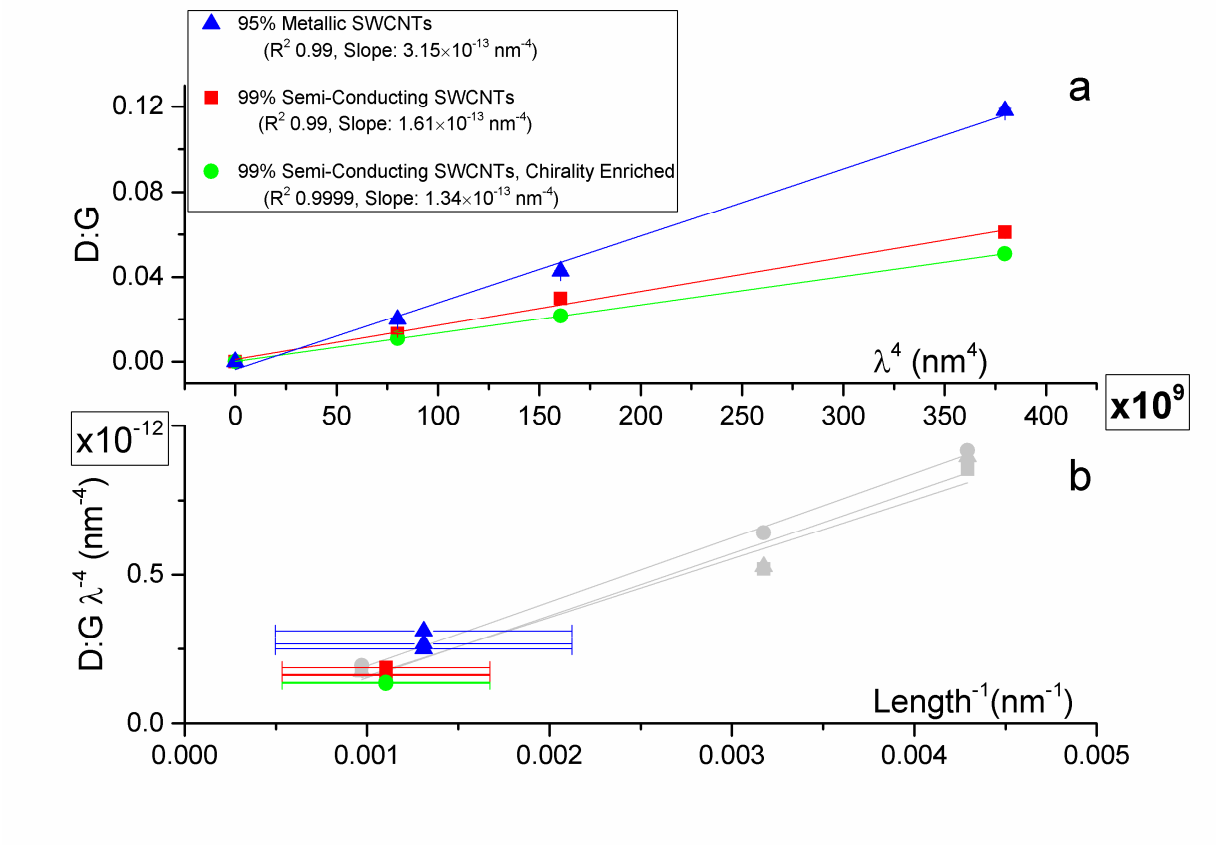

Figure 6| SWCNT films with controlled electronic species concentrations are analysed in the same way as unsorted SWCNT films. **a,** D:G values plotted against λ^4 also show good linearity despite some wavelengths hitting resonant conditions. **b,** The electronic species enriched films also fall on the master curve, supporting that electronic species concentration does not alter D:G's dependence on wavelength and length, at least not in bulk, heavily bundled situations.

4.3 Aligned CNT textile. We have showed that that the D:G ratio in a bulk SWCNT material has a response consistent with λ^4 proportionality and CNT length inverse proportionality, seemingly independent of electronic species concentration and chirality dependent resonances. Now we consider a more complicated textile where the CNTs are at least partly aligned and substantially longer than the probing laser spot. Perhaps more importantly, disordered multiwall CNTs and amorphous carbon are more abundant in the as-is material and we will consider the effects on the D:G ratio to wavelength response when these disordered carbons are removed.

Figure 7 shows D:G values against λ^4 for several aligned CNT textiles: as-is (black) and after the post-process purification (blue and red). Purified material shows good linearity with λ^4 and the

as-is material does not. Even the best fit line to the as-is material has a significant non-zero intercept.

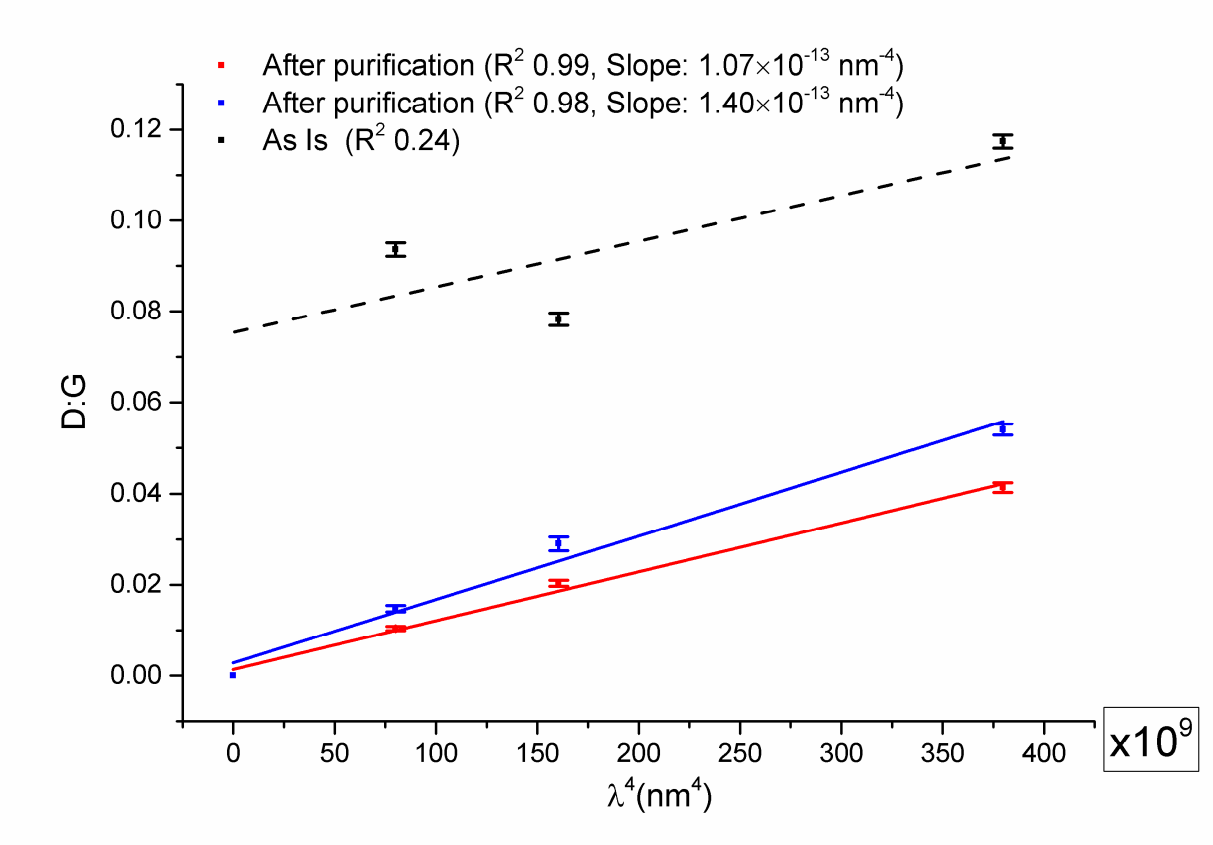

Figure 7| For the aligned CNT textile, D:G values plotted against λ^4. As-is material does not yield a good fit and has a significant non-zero intercept. After purification however, λ^4 dependence is obtained.

Looking at the alignment enhancement between the as-is and purified material (supplemental information, figures S6 to S9), the as-is material's poor linearity and non-zero intercept could be assigned, at first glance, to lack of good microstructure alignment. The D peak after all is a polarization sensitive signal. Note however, that the Raman laser and collection back to the detector were both unpolarised. More importantly, good adherence to λ^4 was demonstrated by the completely unaligned SWCNT films above. The as-is material's poor linearity and non-zero intercept could also be assigned to sample heating and broadening of the G peak, although this is not the case. We verified we were operating with the lowest practical fluence parameters that did

not significantly alter the G peak width. We also took measures to increase thermal contact with the underlying aluminium substrate; this too did not help.

Considering that the purified material does follow λ^4, we assign the as-is non-compliance to the presence of the multiwall CNTs and disordered carbons that was present in the transmission electron microscopy (See supplemental information, figures S6 to S14). This is consistent with our observation (not shown) that the absolute Raman signal magnitude of the purified material is approximately four times that of the as-is material; it has been established that pure graphitic, sp^2 materials have substantially larger Raman cross section than carbon materials with an sp^3 component [7]. In addition, for disordered carbons, the D:G ratio wavelength relationship in general is complex, non-monotonic, and depends greatly on the disordered carbon's exact nature (for example, the degree of hydrogenation and the sp^2 to sp^3 ratio) [19]. Thus, the presence of disordered carbons explains why the as-is material does not follow the λ^4 dependence.

Purified material does show proportionality between the D:G ratio and λ^4. If we take their slopes and apply them to the master curve for the unaligned SWCNT films, the standard purification procedure yields an average characteristic length of 1.6 μm and 2 μm. Considering that the CNTs themselves are significantly longer than these values, this implies that point defects are indeed acting as crystal grain boundaries. Use of this master curve should be made with caution as we do not fully understand its universality, although at this stage it appears independent of electronic species concentration.

4.4 Large laser spot. Using typical microscope objectives, the Raman spectrometer's laser spot is substantially smaller than the average CNT length in our aligned textiles. This implies that the contribution to the D peak signal from CNT ends are not being adequately sampled and this may become problematic as the push to higher conductivity leads to greater CNT lengths with greater graphitic crystallinity. One solution is to simply use a Raman laser beam much larger than the CNT length. This could be accomplished by taking Raman measurements out of focus, although this very quickly leads to weak and unusable Raman signals and we found this did not lead to reliable results. Another possible solution to generate a larger spot is to collect spectrums over many smaller spots, using a commonly applied automated mapping feature, and add the absolute value of the spectra together. Typically, only relative or normalized features in Raman spectra

are considered and, in practice, adding together absolute valued spectra could be problematic because they are more sensitive to instrument and atmospheric perturbations [8].

Instead of a mapping approach or using an out of focus laser beam, we used a specially designed Raman system with a millimeter scale laser spot. This is a laser diameter well beyond the CNT length in our textile and to the best of our knowledge has not been applied to address the issue of adequate sampling of CNT ends or caps in CNT textiles. Figure 8 shows representative, large spot size spectra for a 785 nm excitation on two materials: 1) the as-is aligned CNT textiles, and 2) after the post-process purification. In addition to the large spot size spectra, there are also two spectra taken with the 4x microscope objective with different laser fluences. As shown, while there is some noise, the D peaks from the various spot sizes coincide without significant deviation. This implies that the laser spot size from the 4x objective adequately samples the defects in these CNTs.

Spot size however does appear to affect the width of the G peak. The spectra with the highest fluence has the greatest G peak width while the spectra from the large spot size, with about thirty thousand times smaller fluence, has the lowest G peak width. Fluence based broadening of the G peak is known to originate from heating [40] and highlights that proper D:G calculation requires sufficient mitigation of Raman laser heating effects.

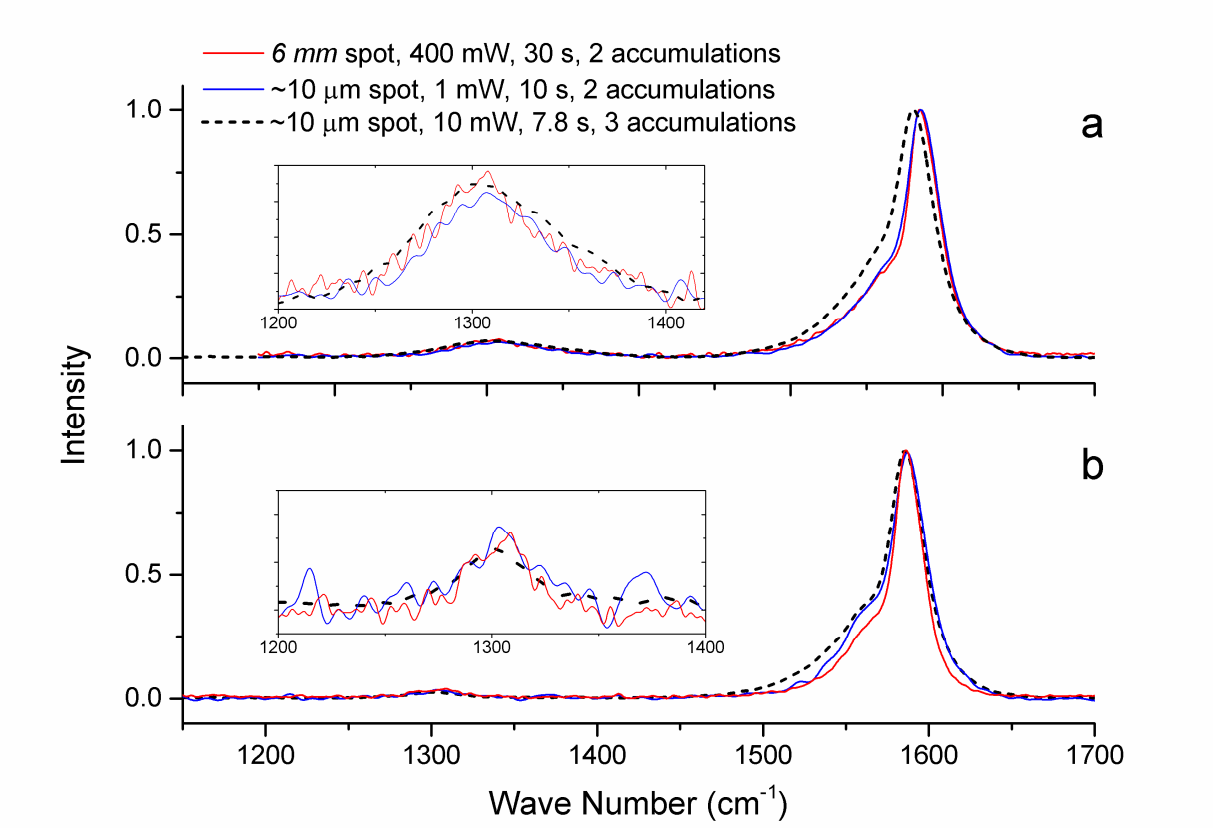

Figure 8| Raman spectra of the 6 mm wide laser spot with the 785 nm laser line for **a,** the as-is aligned CNT textile and **b,** this material after purification. For comparison, spectra from the 4x objective are also provided. Note that these CNTs are known to approach ~1 mm in length, which is far longer than the diameters of typical Raman laser spots.

At this point in material development, the large 6 mm spot size does not yield inherently different Raman spectra than the smaller objectives. A possible explanation is that CNT point defects and CNT end caps have a similar Raman response for CNTs of small diameters. If these long length CNTs textiles could be made nearly defect free such that the CNT ends were the primary source of the D peak signal, then accurate measuring of the D:G value may require a Raman laser spot substantially larger than the SWCNT length.

5. Conclusion

Using purified, unaligned SWCNT films as a standardized material, we demonstrated D:G ratio proportionality to λ^4 and behaviour consistent with inverse proportionality to CNT length, supporting that SWCNT ends act as crystal grain boundaries. These observations resemble the well-established behaviour found in crystalline graphite and graphene, and prevail despite chirality dependent resonances we observe under different laser excitations and with different electronic species concentrations. While these films are pure and in a dense, bundled state, SWCNTs in a more isolated state have been shown not to follow simple power law behaviour for these reasons. We saw that across the different laser lines, averaged lengths, and electronic species concentrations, all curves collapsed into a master curve. The degree of universality of this master curve needs to be explored, such as the effects from doping, bundling, and internal alignment. This could become a useful tool for rapidly turning D:G values into a characteristic crystal length of CNT textiles.

As demonstrated by the as-is aligned CNT textiles however, presence of defective multiwall CNTs and amorphous carbon throws off the power law behaviour. In the context of developing CNT based textiles, the degree of purity would need to be demonstrated by observing if the material's D:G ratio follows λ^4. Once this is demonstrated, changes in D:G / λ^4 slope could be interpreted as changes in the CNT's characteristic crystal length *L*. As CNT lengths grow and point defects become less numerous, D:G characterization of CNT textiles will become increasingly challenging as the D peak's signal to noise ratio competes with the low laser fluence required to minimize sample heating. This problem can be mitigated with using longer excitation wavelengths and larger excitation spot sizes. The 6 mm wide Raman laser beam at 785 nm is an exceptional tool addressing these issues. With even further crystallinity enhancement, as found with graphite and carbon fiber development decades ago [17] [41], the D peak may disappear under the noise floor.

Acknowledgements

We would like to thank Fiona Smail of University of Cambridge Department of Engineering and Stefanie Kreft of University of Cambridge Department of Materials Science and Metallurgy for useful discussions and careful proofreading. We thank John Andrews and Paul Dallin of Clairet Ltd., U.K. for assistance with the large Raman spot size capability. We also thank Andrea Ferrari of University of Cambridge Department of Engineering for valuable conversation.

Works Cited

[1] M. Inagaki, "Applications of graphite intercalation compounds," *J. Mater. Res.,* vol. 4, no. 6, p. 1560, 1989.

[2] A. B. Kaiser, "Electronic transport properties of conducting polymers and carbon nanotubes," *Rep. Prog. Phys. ,* vol. 64 , p. 1–49, 2001.

[3] N. Behabtu, C. C. Young, D. E. Tsentalovich and e. al., "Strong, light, multifunctional fibers of carbon nanotubes with ultrahigh conductivity," *Science,* vol. 339, pp. 182 - 186, 2013.

[4] Y. Zhao, J. Wei, R. Vajtai, P. M. Ajayan and E. V. Barrera, "Iodine doped carbon nanotube cables exceeding specific electrical conductivity of metals," *Sci. Rep.,* vol. 1, no. 83, pp. 1 - 8, 2011.

[5] A. C. Ferrari and D. M. Basko, "Raman spectroscopy as a versatile tool for studying the properties of graphene," *Nat. Nanotechnol. ,* vol. 8, pp. 235 - 246, 2013.

[6] R. Saito, M. Hofmann, G. Dresselhaus, A. Jorio and M. S. Dresselhaus, "Raman spectroscopy of graphene and carbon nanotubes," *Adv. Phys.,* vol. 60, no. 3, pp. 413 - 550, 2011.

[7] M. S. Dresselhaus, A. Jorio, A. S. Filho and R. Saito, "Defect characterization in graphene and carbon nanotubes using Raman spectroscopy," *Phil. Trans. R. Soc. A,* vol. 368, pp. 5355 - 5377, 2010.

[8] R. A. DiLeo, B. J. Landi and R. P. Raffaelle, "Purity assessment of multiwalled carbon nanotubes by Raman spectroscopy," *J. Appl. Phys,* vol. 101, p. 064307, 2007.

[9] J. Pöhls, et al., "Physical properties of carbon nanotube sheets drawn from nanotube arrays," *Carbon,* vol. 50, no. 11, p. 4175–4183, 2012.

[10] D. Mattia, et al., "Effect of graphitization on the wettability and electrical conductivity of CVD-carbon nanotubes and films," *J. Phys. Chem. B ,* vol. 110, pp. 9850-9855, 2006.

[11] R. Rao, J. Reppert, R. Podila, X. Zhang, A. M. Rao, S. Talapatra and B. Maruyama, "Double resonance Raman study of disorder in CVD-grown single-walled carbon nanotubes," *Carbon,* vol. 49, p. 1318 – 1325, 2011.

[12] J. A. Fagan, J. R. Simpson, B. J. Bauer, S. H. D. P. Lacerda, M. L. Becker, J. Chun, K. B. Migler, A. R. H.

Walker and E. K. Hobbie, "Length-dependent optical effects in single-wall carbon nanotubes," *J. Am. Chem. Soc.,* vol. 129, pp. 10607 - 10612, 2007.

[13] S. G. Cou, H. S. J. Kong, A. J. R. Saito, M. Zheng, G. Dresselhaus and M. Dresselhaus, "Length characterization of DNA-wrapped carbon nanotubes using Raman Spectrocopy," *Appl. Phys. Lett.,* vol. 90, p. 131109, 2007.

[14] J. R. Simpson, J. A. Fagan, M. L. Becker, E. K. Hobbie and A. R. H. Walker, "Length-dependent Raman spectroscopy of single-walled carbon nanotubes: the effect of dispersant on defects," *Condens. Mater.,* pp. 1 - 3, 2008.

[15] L. Zhang, H. Li, K.-T. Yue, S.-L. Zhang, X. Wu, J. Zi, Z. Shi and Z. Gu, "Effects of intense laser irradiation on Raman intensity features of carbon nanotubes," *Phys. Rev. B,* vol. 65, p. 073401, 2002.

[16] Y. Miyata, K. Mizuno and a. H. Kataura, "Purity and defect characterization of single-wall carbon nanotubes using Raman spectroscopy," *J. Nanomat.,* p. 786763, 2011.

[17] F. Tuinstra and J. L. Koenig, "Raman spectrum of graphite," *J. Chem. Phys,* vol. 53, pp. 1126 - 1130, 1970.

[18] L. G. Cançado, K. Takai, T. Enoki, M. Endo, Y. A. Kim, H. Mizusaki, A. Jorio, L. N. Coelho, R. Magalhães-Paniago and M. A. Pimenta, "General equation for the determination of the crystallite size La of nanographite by Raman spectroscopy," *Appl. Phys. Lett.,* vol. 88, p. 163106, 2006.

[19] A. C. Ferrari and J. Robertson, "Resonant Raman spectroscopy of disordered, amorphous, and diamondlike carbon," *Phys. Rev. B,* vol. 64, p. 075414, 2000.

[20] K. Sato, R. Saito, Y. Oyama, J. Jiang, L. Cancado, M. Pimenta, A. Jorio, G. Samsonidze, G. Dresselhaus and M. Dresselhaus, "D-band Raman intensity of graphitic materials as a function of laser energy and crystallite size," *Chem. Phys. Lett.,* vol. 427, no. 1, pp. 117 - 121, 2009.

[21] L. Cançado, A. Jorio, E. M. Ferreira, F. Stavale, C. Achete, R. Capaz, M. Moutinho, A. Lombardo, T. Kulmala and A. Ferrari, "Quantifying defects in graphene via Raman spectroscopy at different excitation energies," *Nano Lett.,* vol. 11, no. 8, p. 3190 – 3196, 2011.

[22] S.D.M. Brown, et al., "Observations of the D-band feature in the Raman spectra of carbon nanotubes," *Physical Review B,* vol. 64, p. 073403, 2001.

[23] A. Lopez-Lorente, B. M. Simonet and M. Valcarcel, "Raman spectroscopic characterization of single walled carbon nanotubes: influence of the sample aggregation state," *Analyst,* vol. 130, pp. 290 - 298, 2014.

[24] D. A. Heller, P. W. Barone, J. P. Swanson, R. M. Mayrhofer and M. S. Strano, "Using Raman

spectroscopy to elucidate the aggregation state of single-walled carbon nanotubes," *J. Phys. Chem. B,* vol. 108, pp. 6905 - 6909, 2004.

[25] M. J. O'Connell, S. M. Bachilo, C. B. Huffman, V. C. Moore, M. S. Strano, E. H. H. K. L. Rialon, P. J. Boul, W. H. Noon, C. Kittrell, J. Ma, R. H. Hauge, R. B. Weisman and R. E. Smalley, "Band gap fluorescence from individual single-walled CNT," *Science,* vol. 297, pp. 593 - 596, 2002.

[26] M. S. Dresselhaus, D. Dresselhaus, P. Avouris. Carbon Nanotubes: Synthesis, Structure, Properties, and Applications, Springer, 2001.

[27] G. D. Saraiva, A. G. S. Filho, G. Braunstein, E. B. Barros, J. M. Filho, E. C. Moreira, S. B. Fagan, D. L. Baptista, Y. A. Kim, H. Muramatsu, M. Endo and M. S. Dresselhaus, "Resonance Raman spectroscopy in Si and C ion-implanted double-wall carbon nanotubes," *Phys. Rev. B,* vol. 80, p. 155452, 2009.

[28] K. Koziol, J. Vilatela, A. Moisala, M. Motta, P. Cunniff, M. Sennett and A. Windle, "High-performance carbon nanotube fiber," *Science,* vol. 318, pp. 1892 - 1895, 2007.

[29] S. Wang, et al. "Statistical characterization of single-wall carbon nanotube length distribution," *Nanotechnology,* vol. 17, p. 634–639, 2006.

[30] M. S. Arnold, A. A. Green, J. F. Hulvat, S. I. Stupp and M. C. Hersam, "Sorting carbon nanotubes by electronic structure using density differentiation," *Nat. Nanotechnol.,* vol. 1, pp. 60 - 66, 2006.

[31] M. Engel, et al. "Thin film nanotube transistors based on self-assembled, aligned, semiconducting carbon nanotube arrays," *ACS Nano,* vol. 2, no. 12, p. 2445–2452, 2008.

[32] T.S. Gspann, et al. "High thermal conductivities of carbon nanotube films and micro-fibres and their dependence on morphology," *Carbon,* vol. 114, pp. 160-168, 2017.

[33] A.G. Rinzler, et al. "Large-scale purification of single-wall carbon nanotubes: process, product, and characterization," *Appl. Phys. A ,* vol. 67, p. 29–37 , 1998.

[34] H. Kajiura, et al. "High-quality single-walled carbon nanotubes from arc-produced soot," *Chemical Physics Letters ,* vol. 364 , p. 586–592, 2002.

[35] C. Fabbro, et al. "Local ''repristinization'' of oxidized single-walled carbon nanotubes by laser treatment," *Carbon,* vol. 76, pp. 96-104, 2014.

[36] P. Corio, et al. "Evolution of the molecular structure of metallic and semiconducting carbon nanotubes under laser irradiation," *Chemical Physics Letters ,* vol. 360, p. 557–564, 2002.

[37] N. Souza, et al "In situ tracking of defect healing and purification of single-wall carbon nanotubes with laser radiation by time-resolved Raman spectroscopy," *RSC Adv.,* vol. 5, p. 62149–62159, 2015.

[38] F. Huang, K. T. Yue, P. Tan, S.-L. Zhang, X. Z. Zujin Shi and Z. Gu, "Temperature dependence of the Raman spectra of carbon nanotubes," *J. Appl. Phys.,* vol. 84, no. 7, pp. 4022 - 4024, 1998.

[39] H. Li, K. Yue, Z. L. Lian, Y. Zhan, L. X. Zhou, S. Zhangb, Z. Shi, Z. Gu, B. Liu, R. Yang, H. Yang, G. Zou, Y. Zhang and S. Iijima, "Temperature dependence of the Raman spectra of single-wall carbon nanotubes," *Appl. Phys. Lett.,* vol. 76, no. 15, pp. 2053 - 2055, 1999.

[40] X. Zhang, F. Yang, D. Zhao, L. Cai, P. Luan, Q. Zhang, W. Zhou, N. Zhang, Q. Fan, Y. Wang, H. Liu, W. Zhou and S. Xie, "Temperature dependent Raman spectra of isolated suspended single-walled carbon nanotubes," *Nanoscale,* vol. 6, pp. 3949 - 3953, 2014.

[41] T. C. Chieu, G. Timp, M. S. Dresselhaus, M. Endo and A. W. Moore, "High-field magnetoresistance measurements on highly ordered graphite fibers," *Phys. Rev. B,* vol. 27, no. 6, pp. 3686 - 3697, 1983.